Shear velocity structure of the crust and upper mantle of Madagascar derived from surface wave tomography

Martin A Pratt, Michael A Wysession, Ghassan A Aleqabi, Douglas D Wiens, Andrew A Nyblade, Patrick A Shore, Gérard A Rambolamanana, Fenitra A Andriampenomanana, Tsiriandrimanana A Rakotondraibe, Robert D Tucker, et al.

Shear velocity structure of the crust and upper mantle of Madagascar derived from surface wave tomography

Martin J. Pratt [a,*], Michael E. Wysession [a], Ghassan Aleqabi [a], Douglas A. Wiens [a], Andrew A. Nyblade [b], Patrick Shore [a], Gérard Rambolamanana [c], Fenitra Andriampenomanana [c], Tsiriandrimanana Rakotondraibe [c], Robert D. Tucker [d], Guilhem Barruol [e], Elisa Rindraharisaona [f]

[a] *Washington University in St. Louis, MO, USA*
[b] *Pennsylvania State University, State College, PA, USA*
[c] *Institut Observatoire et Geophysique d'Antananarivo, Madagascar*
[d] *University of Maryland, College Park, MD, USA*
[e] *Laboratoire GéoSciences Réunion, Université de la Réunion, Institut de Physique du Globe de Paris, UMR CNRS 7154, Université Paris Diderot, F-97744 Saint Denis, France*
[f] *Deutsches GeoForschungsZentrum (GFZ), Germany*

ARTICLE INFO

Article history:
Received 16 July 2016
Received in revised form 15 October 2016
Accepted 21 October 2016
Available online 22 November 2016
Editor: P. Shearer

Keywords:
surface wave
ambient noise
tomography
Madagascar
intraplate volcanism

ABSTRACT

The crust and upper mantle of the Madagascar continental fragment remained largely unexplored until a series of recent broadband seismic experiments. An island-wide deployment of broadband seismic instruments has allowed the first study of phase velocity variations, derived from surface waves, across the entire island. Late Cenozoic alkaline intraplate volcanism has occurred in three separate regions of Madagascar (north, central and southwest), with the north and central volcanism active until <1 Ma, but the sources of which remains uncertain. Combined analysis of three complementary surface wave methods (ambient noise, Rayleigh wave cross-correlations, and two-plane-wave) illuminate the upper mantle down to depths of 150 km. The phase-velocity measurements from the three methods for periods of 8–182 s are combined at each node and interpolated to generate the first 3-D shear-velocity model for sub-Madagascar velocity structure. Shallow (upper 10 km) low-shear-velocity regions correlate well with sedimentary basins along the west coast. Upper mantle low-shear-velocity zones that extend to at least 150 km deep underlie the north and central regions of recent alkali magmatism. These anomalies appear distinct at depths <100 km, suggesting that any connection between the zones lies at depths greater than the resolution of surface-wave tomography. An additional low-shear velocity anomaly is also identified at depths 50–150 km beneath the southwest region of intraplate volcanism. We interpret these three low-velocity regions as upwelling asthenosphere beneath the island, producing high-elevation topography and relatively low-volume magmatism.

1. Introduction

Though Madagascar is a large island with a geologic history extending far back into the Archean (Collins, 2006; Tucker et al., 2011), its crust and mantle structure have been largely unexplored by seismic methods until now. Despite recent surface geologic mapping, culminating in the high-resolution geologic map of Roig et al. (2012), the lack of subsurface observations has prevented an accurate interpretation of the geologic and tectonic histories of the region. For example, prior to the current studies, the crustal thickness of the island had only been inferred from a gravity survey (Fourno and Roussel, 1994) and more recently by receiver function techniques applied at the few permanent seismic stations (Rindraharisaona et al., 2013).

One of the more unusual aspects of Madagascan geology is the occurrence of several episodes of Cenozoic volcanism in the central (Itasy/Ankaratra) and northern regions (Nosy Be/Massif D'Ambre) of the island (Emerick and Duncan, 1982; Nougier et al., 1986; Tucker and Conrad, 2008) (Fig. 1). These two regions have been

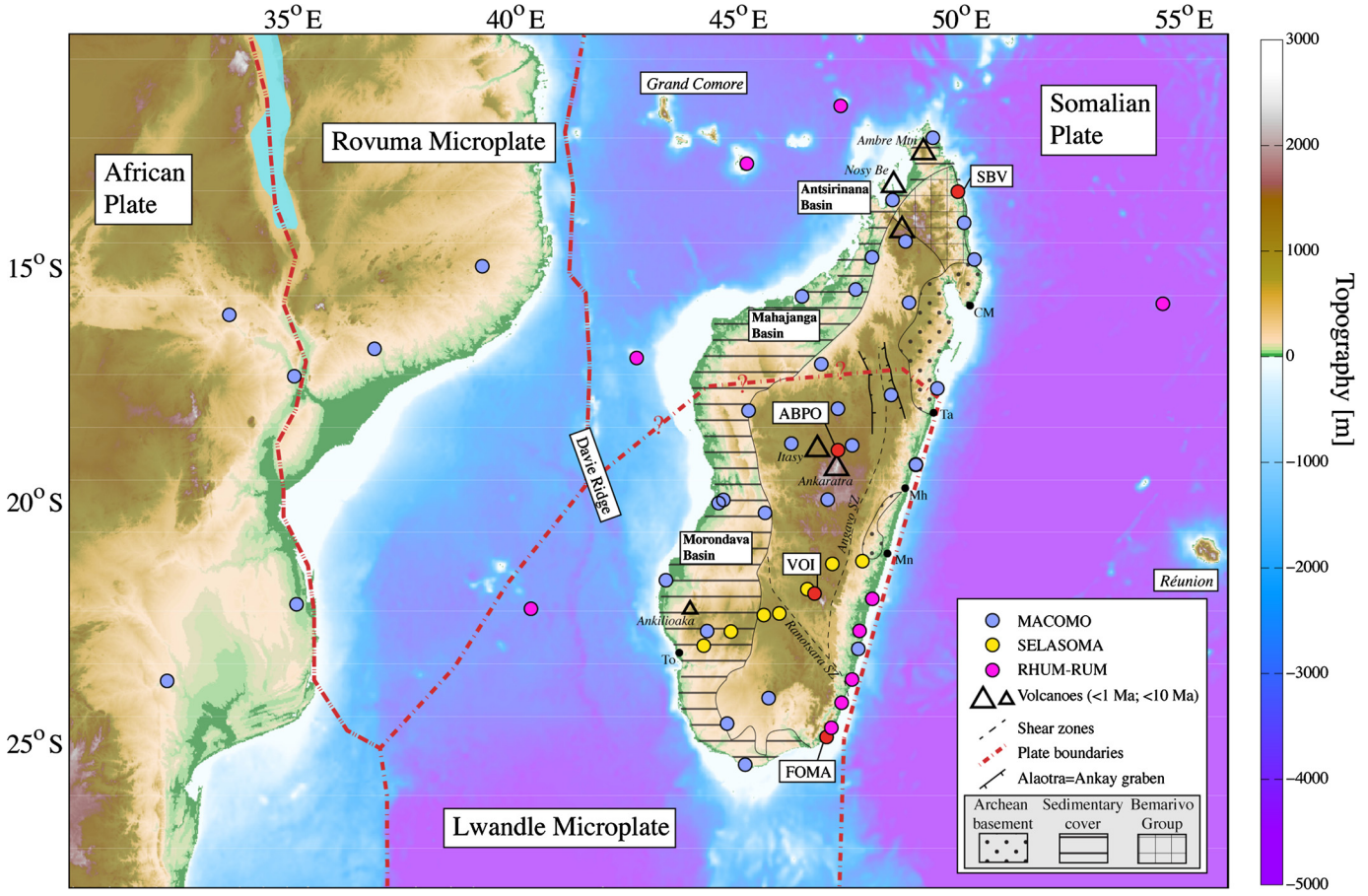

Fig. 1. Topographic map of the Madagascar/Mozambique region. Simplified geology for Madagascar is adapted from Roig et al. (2012), showing Precambrian metamorphic terranes consisting of Archean cratonic fragments, the Bemarivo Group, and the untextured Antananarivo Group. Phanerozoic sediments cover much of the west of Madagascar. Cenozoic volcanic areas are as marked, as are Precambrian shear zones and the post-Miocene Alaotra–Ankay graben structure. Initials are place names referred to in the text: A – Antananarivo, CM – Cap Masoala, Mh – Mahanoro, Mn – Mananjary, Ta – Tamatave, To – Toliara. Station locations are shown for the MACOMO, RHUM-RUM, and SELASOMA seismic projects used in this study. Known active hotspots currently lie beneath Grande Comore and Réunion. The Davie ridge is an inferred transform fault controlling the relative movement of Madagascar with respect to Africa during the Mesozoic. Plate boundaries are after Stamps et al. (2015). Elevation and bathymetry are from ETOPO1 (Amante and Eakins, 2009). (For interpretation of the colors in this figure, the reader is referred to the web version of this article.)

referred to in the literature as the Northern Madagascar Alkaline Province (NMAP) and the Central Madagascar Alkaline Province (CMAP). A third outcrop of late Cenozoic volcanism was also identified in the southwestern part of the island by Bardintzeff et al. (2010), which we will refer to as the SMAP. Several ideas have previously been put forward to explain this anomalous volcanic activity (Emerick and Duncan, 1982; Nougier et al., 1986). However, without the imaging provided by broadband seismological investigations, hypotheses concerning the origin of this magmatic activity could not be tested. It was in the context of this challenge that the seismic imaging presented here was carried out through the 2-year deployment of an island-wide network of 26 broadband seismometer locations, complemented by six seismometers deployed in neighboring Mozambique as part of the MACOMO (MAdagascar COmores MOzambique) experiment (Wysession et al., 2011). The experiment was simultaneously accompanied by the German SELASOMA seismic deployment of twenty-seven broadband stations along a SW–NE profile in the south of Madagascar (Tilmann et al., 2012) and by terrestrial deployments of ten broadband stations in the frame of the RHUM-RUM experiment; five along the SE coast of Madagascar and five in the surrounding Eparses Islands (Barruol and Sigloch, 2012).

Previous broadband seismological work within Madagascar was carried out using four permanent broadband seismometer stations at ABPO (GSN), FOMA (GEOSCOPE), SBV and VOI (GEOFON) (Rindraharisaona et al., 2013). Small deployments of short-period seismometers were also carried out by researchers from the University of Antananarivo, through these short-period sensors were only sensitive to local seismicity in the Itasy and Ankaratra region (e.g. Rindraharisaona et al., 2013), and were not able to resolve deep and large-scale structures. The global model Crust1.0 (Laske et al., 2013) includes a representation of Madagascar with a 1° parameterization that varies between a maximum crustal thickness of ∼42 km along the backbone of the island, where the topography is highest, to a minimum crustal thickness of ∼30 km along the western coast. This model improved upon crustal-thickness models that were based on gravity studies, which suggested crustal-thickness variations of 25–35 km (Rakotondraompiana et al., 1999). Upper mantle observations beneath Madagascar had previously only been constrained by receiver-function and teleseismic surface-wave shear-velocity inversions for each of the four permanent stations (Rindraharisaona et al., 2013), which also concluded that the Madagascan lithosphere is relatively thin compared with East Africa, and that the lowest asthenospheric shear velocities lie beneath some of the highest topography around the central Itasy region.

In this study, we utilize an island-wide deployment of seismometers that is able to explore the crust and upper mantle seismic velocities of Madagascar using phase velocity measurements derived from both ambient noise and teleseismic surface wave analyses, providing good structural resolution to depths of up to 200 km. Resolving below this depth will require a subse-

quent analysis of teleseismic body wave tomography. We apply a linearized shear-velocity inversion to the measured phase velocities to produce the first complete regional shear-velocity model of Madagascar.

2. Geologic setting

Madagascar has an unusual geologic history that has primarily shaped its crustal and lithospheric structures through a Pan-African amalgamation of Precambrian terranes that were positioned at the suture of Eastern and Western Gondwana (Collins, 2006, and the references therein). These tectonic terranes include a fragment of the Archean Western Dharwar craton (Antongil–Masaora Terrane along the eastern coast) (Pacquette et al., 2003), which is a series of Proterozoic terranes containing remnant shear zones (Antananarivo terrane, throughout the Madagascan highland plateaus) (Fig. 1) (Tucker et al., 2007, and the references therein).

Madagascar rifted away from Africa along with India ~165–130 Ma, during the break-up of Gondwana (Rabinowitz et al., 1983; Coffin and Rabinowitz, 1987). Throughout this time, volcanic rocks were emplaced across many regions of Madagascar (Fig. 1). This rifting thinned the crust along the west coast of Madagascar, allowing syntectonic sedimentary basins to form there. The east coast of Madagascar was shaped by the subsequent rifting of the Indian subcontinent that moved northwards along a transform fault from 95 Ma to 84 Ma (e.g., Gibbons et al., 2013), and the whole island has remained tectonically stable since then.

Madagascar was subject to widespread flood basalts (now found at the surface primarily around the periphery of the island) that erupted voluminously but briefly during this time, ~95–85 Ma ago, and may have once covered the island (Storey et al., 1995). This is commonly linked to the migration of Madagascar/India over the Marion hot spot (Storey et al., 1995; Torsvik et al., 1998), leading to fracturing of the overriding plate, rapid emplacement of mantle-derived tholeiitic basalt and crustal-derived dacite/alkali rhyolite magmas, and eventual fragmentation of India from Madagascar.

The enigmatic igneous provinces of much more recent alkaline intraplate volcanism, including the large NMAP (3800 km^2) and CMAP (6000 km^2) areas, are shown in Fig. 1. Radiometric $^{40}Ar/^{39}Ar$ ages show that the igneous rocks are principally 25–1 Ma old (Emerick and Duncan, 1982; Nougier et al., 1986; Tucker and Conrad, 2008), but began as early as 50 Ma. In certain regions of the north (around Nosy Be and the Massif d'Ambre) and in the center of the island (in the Itasy and Ankaratra regions west of the capital, Antananarivo) volcanism has extended into the Holocene (Collins, 2006). The SMAP volcanic activity, found in a comparatively small region of southwestern Madagascar, near Toliara, has isotopic ages of ~9 Ma, similar to some of the CMAP volcanics (Bardintzeff et al., 2010).

A first hypothesis to explain the Madagascan intraplate volcanism connects it to the more active Comoros volcanic alignment to the northwest (Emerick and Duncan, 1982), which extends SE-to-NW from Mayotte Island to the Grande Comore Island and the active Karthala volcano. A second hypothesis relates both the Comoros and Madagascar volcanism to the southern termination of the East African Rift and to the eastward motion of the Somalian plate relative to Nubia. Although the geometry of the southern termination of the Somalian plate is still debated (Saria et al., 2014; Stamps et al., 2015), the diffuse termination of the East African Rift may extend through the Comoros volcanic alignment and into the intraplate Madagascar volcanism (Michon, 2016). A third hypothesis could involve deep connections to a lower mantle African superplume (Ebinger and Sleep, 1998), which would generate a large-scale mantle upwelling (Forte et al., 2010) that spreads radially in the upper mantle beneath Southern Africa. This upwelling could bring hot asthenospheric mantle to the Mozambique Channel region, generating volcanism within Madagascar. A fourth hypothesis involves fracture zones created during continental separation (Nougier et al., 1986). These bands of weakness may be reactivated through periods of regional lithospheric extension, allowing local asthenospheric upwelling and volcanic activity. The regional fracture zones have a similar orientation to the N–S trending Davie Ridge, believed to be the transform fault guiding Madagascar southwards during the Cretaceous (Coffin and Rabinowitz, 1987) and which has been the site of recent seismic reactivation (Grimison and Chen, 1988). Similarly orientated remnant structures from the amalgamation of Madagascar in the Precambrian, such as the Ranotsara shear zone, may also provide areas of crustal and/or lithospheric weakness for tectonic extension to exploit. These four hypotheses are not completely independent and may interact concurrently to produce intraplate volcanism.

At regional scales, seismicity is clearly aligned along the Davie Ridge, along the Comoros volcanic alignment and beneath Madagascar. Seismicity within Madagascar shows highest concentrations in the center of the island (Rindraharisaona et al., 2013, and the references therein). The majority of these small (<M4) events have extensional focal mechanisms, reflecting a regional E–W extensional stress regime (Grimison and Chen, 1988; Rindraharisaona et al., 2013), which suggests that the whole region may correspond to a diffuse, extensional plate boundary. The seismicity appears to align in bands approximately N140E that align with mapped normal fault structures and are often associated with the occurrence of hot springs, suggesting high regional heat-flow rates. Rindraharisaona et al. (2013) also used a joint inversion of receiver functions and surface waves to study the upper mantle at the sites of the four permanent stations. They found that the center of the island, beneath the Global Seismic Network (GSN) station ABPO, is underlain by relatively seismically slow upper mantle material, which may suggest an asthenospheric upwelling in this region, although both the spatial and depth extent of the feature was not well resolved.

Tectonic studies of the CMAP and Alaotra–Ankara graben system have shown that these areas are actively extending, resulting in high erosional gullies known locally as lavakas. In places, these features cut into Neogene rocks suggesting that uplift may have been occurring for the past 10–15 Ma (Cox et al., 2010). The topography of Madagascar is unusually elevated for old, continental crust, with large areas of the central and northern parts of the island generally elevated ~1 km above sea level, but more than 2 km in places. This is especially unusual considering that Madagascar is unlikely to have experienced extensive compressional tectonics since at least ~140 Ma ago, following its separation from Africa (e.g., Rabinowitz et al., 1983). Examinations of river profiles have suggested that Madagascar has experienced active uplift since the early Miocene (Roberts et al., 2012). Comparisons can be made to other uplifted broad plateaus such as the Massif Central in France (Chevrot et al., 2014), which has also undergone recent intraplate volcanism, and the Hangay Dome of Mongolia (e.g., Petit et al., 2008), where crustal thickness is 40–50 km and the elevation may be accommodated by a thinner lithosphere.

3. Data and methods

The MACOMO project deployed 36 broadband instruments (9 Guralp CMG-3Ts, 10 Trillium 120PAs, 17 Streckeisen STS-2s, each with a Quanterra Q330 datalogger) at 26 locations within Madagascar (including some repeat locations due to instrument failures) and at 6 locations within Mozambique. Broadband seismometers were operated for two years at 10 Madagascar locations, starting in October 2011, supplemented by an additional 16 broadband stations that operated for one year, starting in August 2012. All stations were removed in August 2013 and data are available

at the IRIS data management center under code XV (Wysession et al., 2011). Contemporaneous with the MACOMO deployment were two other regional broadband deployments. The RHUM-RUM (Réunion Hotspot and Upper Mantle–Réunions Unterer Mantel) project mainly deployed ocean bottom seismographs to the east and south of Madagascar, but also installed five land stations in southeastern Madagascar and five island stations on the Iles Eparses around Madagascar. RHUM-RUM data is under the FDSN code YV at the French RESIF data portal and will be publically available at the end of 2017 (http://seismology.resif.fr) (Barruol and Sigloch, 2012). In addition, the Seismological Signatures in the Lithosphere/Asthenosphere system of Southern Madagascar (SELASOMA) experiment installed 25 broadband stations in a linear deployment across southern Madagascar to examine the crustal structure of Madagascar as it crosses the Ranotsara shear zone and other tectonic features (FDSN network code ZE 2012–2014; Tilmann et al., 2012). These stations fill the gaps in the MACOMO station coverage. The present study uses the 10 RHUM-RUM land and island stations, 7 of the SELASOMA broadband stations and the 4 permanent broadband stations deployed on Madagascar: ABPO (IU GSN, 2007–present); VOI and SBV (GE GEOFON, 2009–present; GEOFON Data Center (1993)); and FOMA (G GEOSCOPE, 2008–present) (see Fig. 1 and Supplementary Table S1).

Three complementary methods are used to analyze surface wave phase velocities:

1) Ambient noise tomography, following Bensen et al. (2007), is used over relatively short periods (0–40 s) and is therefore best for shallow (upper 30 km) investigations.
2) A station-to-station cross-correlation approach recently developed by Jin and Gaherty (2015) is used for the intermediate period range of 20–100 s.
3) The two-plane-wave analysis of Yang and Forsyth (2006) is used over a period range of 18–182 s, which provides good resolution to depths of 150–200 km.

The phase-velocity dispersion observations from these three methods are combined at each nodal point of the model and inverted for a three-dimensional shear-velocity model using the methodology of Herrmann and Ammon (2002).

3.1. Ambient noise tomography

Now a standard seismological technique, ambient noise tomography (ANT) relies upon the observation that the average seismic noise field reveals surface-wave particle motions with propagation velocities that are frequency-dependent (e.g., Larose et al., 2005). Seismic ground noise records from a station pair can be cross-correlated to furnish an approximation of the elastic impulse response (Green's function) as if one of the stations is a virtual source. Rayleigh wave dispersive properties of the extracted Green's functions from cross-correlations of ambient-noise records at two stations or more are used to produce tomographic images (e.g., Shapiro and Campillo, 2004).

The method of Bensen et al. (2007) is followed here, using vertical-component time series from 1 July 2011 to 1 August 2013. The instrument responses are removed from the time series, which are then cut into 12-hr windows with an overlap of 8 hr. The time series windows are cross-correlated among all stations using a frequency-domain normalization, and then stacked to produce station-to-station Green's functions from which Rayleigh waves are extracted. The FTAN software package of Levshin et al. (1992) is used to analyze the dispersion of each interstation Green's function. These functions are then mapped over a 0.5° grid of nodes using the tomographic inversion method of Barmin et al. (2001), producing 1-D dispersion curves for phase and group velocities at periods 8–40 s.

3.2. Cross-correlation of teleseismic surface waves

For teleseismic surface waves from earthquake sources, the Automated Surface Wave Phase Velocity Measuring System (ASWMS) of Jin and Gaherty (2015) uses a cross-correlation of fundamental-mode surface waves to calculate station-to-station phase velocities as

$$C(t) = S_1 \star W_s S_2 \tag{1}$$

where S_1 is the seismogram at a particular station, W_S is a window function isolating the surface wave energy at a neighboring station S_2, and $C(t)$ contains the lag information for all coherent signals. $C(t)$ is windowed and narrow-band filtered; low and high cut-off frequencies are ±10% of the center frequencies. The raw phase velocity is found by minimizing the misfit between a predicted wavelet and the narrow-band-filtered cross-correlogram. For the detailed methodology see Jin and Gaherty (2015). This technique has had limited applications to temporary regional deployments such as the combined Madagascar deployment used in this study, and is applied here to provide a test to its potential across such a network.

The data involve Rayleigh-wave observations from 182 teleseismic events of $M_w > 6$ (7 October 2011 to 30 August 2013) that are more than 30° away from Madagascar so that a plane wave assumption is valid (Supplementary Fig. S1). Station pairs chosen for the correlation were limited to 50–500 km in distance to minimize cycle skipping. We produce 2D phase-velocity maps using Eikonal tomography (following references in Jin and Gahery, 2015) at 15 periods between 20 s and 100 s for a series of 0.5° nodes across Madagascar.

3.3. The two-plane-wave method

To extend the phase velocity range to longer periods (out to 182 s), and therefore increase the depth of the model resolution, we apply the two-plane-wave (TPW) method of Yang and Forsyth (2006) to Rayleigh waves from 183 teleseismic events. For a regional surface-wave inversion, the incoming displacement (U) of the Rayleigh wavefield at frequency ω, recorded at a seismic station, can be represented by the sum of two plane waves (Forsyth and Li, 2005):

$$U_z(\omega) = A_1(\omega)e^{-i(\mathbf{k}_1\cdot\mathbf{x}-\omega t)} + A_2(\omega)e^{-i(\mathbf{k}_2\cdot\mathbf{x}-\omega t)} \tag{2}$$

where A and $\mathbf{k}$ are the amplitude and horizontal wavenumber vector of each of the plane waves and $\mathbf{x}$ is a position vector for each station relative to the reference station.

Vertical components of Rayleigh waveforms are narrow-band Butterworth-filtered at twenty-five periods between 18 s and 182 s, in frequency bands of ±10% of the center frequency. The observed fundamental-mode Rayleigh waves are identified and windowed using the 3-D CUB2 velocity model of Ritzwoller et al. (2003). The windows are tapered to minimize edge effects and we apply a quality-control signal-to-noise ratio cut-off of 5. Each window is converted into the frequency domain to obtain amplitude and phase information. The model grid is parameterized with 437 grid nodes with a node spacing of 0.8° at the center of the grid and 1.2° at the edges in order to allow the estimated phase velocities to absorb effects that are not explained by the sum of two plane waves.

The parameters of the incoming two plane waves are first estimated using a simulated annealing method based on the initial phase-velocity model. Second, the plane-wave parameters and

phase-velocity parameters at each node are solved simultaneously with a generalized linear inversion. The model parameters are updated at each iteration and the inversion stops when the maximum number of iterations is reached or the convergence condition is achieved. Following a similar procedure to Li and Burke (2006), we iterate the model values a maximum of 10 times, set the characteristic wavelength for averaging and calculating spatial sensitivity to be 100 km, and assign the *a priori* error for each node velocity to be 0.15 km/s. This allows the model to minimize edge affects caused by a heterogeneity that cannot be represented by two plane waves.

3.4. Combined shear-velocity inversion

The 1-D dispersion curves at each of the model nodes from each of the three different methods of analysis are combined to form a single model. For frequency bands that overlap between the different methods, the resulting maps show general similarities in the overall patterns of phase velocity variations (Supplementary Fig. S2). Differences in phase velocity maps between each method are likely due to ray coverage and interpolation methods implemented by each approach. The method of Herrmann and Ammon (2002) is used to fit the combined dispersion with 1-D vertical velocity models by allowing thin (2–5 km) layers to change in velocity value but not thickness. For overlapping periods of the ASWMS and TPW methods we weight the inversion based on the standard deviation of the observations.

The initial model is loosely based on AK135 (Kennett et al., 1995), with a constant shear velocity throughout the crust and upper mantle of 4.48 km/s and a set of twenty-five 2-km-thick layers. As little knowledge of crustal structure is currently known in Madagascar, we smooth over all layers. The phase-velocity dispersion curves that are calculated for each 1-D model are found to provide an excellent fit after 50 iterations.

A shear-velocity discontinuity is inserted in order to more realistically mimic a Moho velocity increase. We make the assumption that the Moho is consistent throughout Madagascar and equal to 4.125 km/s. This value is based on the only previous study of receiver function analysis in Madagascar using the 4 permanent seismic stations in Madagascar (ABPO, SBV, VOI, FOMA) (Rindraharisaona et al., 2013). We apply a 0.14 km/s jump at this assumed depth of the Moho, accommodating this offset by reducing the shear velocity in the lower crust by 0.042 km/s and raising the upper mantle layer velocities by 0.098 km/s.

The iterative inversion process is run again using the new 1-D models with a Moho velocity step as a starting model. To retain the Moho in the final model, the inversion is run with a higher damping parameter in the layer just below the Moho.

4. Results

4.1. Ambient noise tomography

The ANT spatial resolution tests are determined by forward-modeling a delta function using the process discussed in Section 3.1 (Barmin et al., 2001), and are influenced by the station spacing, with shorter periods requiring a closer station spacing. Results of the resolution tests are shown in Supplementary Fig. S3 and show good spatial resolution of seismic features of $<$50 km width across Madagascar at all periods.

The resulting ANT Rayleigh wave velocities are a product of Earth structure at relatively shallow depths ($\sim$10–50 km), and correlate well with the known surface geology. Fig. 2 shows a subset of phase-velocity slices from the ANT results. At 10 s, which largely samples structures at depths of 2–20 km, there are two notable low-phase-velocity regions ($<$3.15 km/s) on the west coast of Madagascar. A third, small low-velocity region can be seen at the very north end of the island. These three seismic features correlate well with the locations of three sedimentary basins along the west coast. At periods $>$30 s, low phase velocities become concentrated in three regions: the central (CMAP), northern (NMAP), and southwestern (SMAP) provinces. At 20–40 s period, the 2D maps show smearing of the phase velocities over the Mozambique Channel. This is due to limited crossing rays in the channel from the lack of available stations. At these periods, relatively fast velocities are generally observed in the Mozambique Channel compared to Madagascar, as would be expected from the differences in crustal thickness and composition.

4.2. Automated surface wave phase velocity measuring system

For each period band, the consistency of the phase-velocity measurement at each node can be characterized by a standard deviation and is shown in Supplementary Fig. S4. The highest variations in phase velocity occur at shorter periods, suggesting that the limit of resolution has been reached, given the station spacing. Standard deviations of $<$0.1 are found over most of Madagascar for the majority of period bands within 25–100 s.

A subset of the ASWMS phase velocity maps at several different periods are shown in Fig. 3. In the 20 s map, the backbone of the island exhibits relatively low phase velocities when compared with the rest of Madagascar and the surrounding oceanic crustal regions. At phase-velocity periods of 30–40 s, significant low-velocity regions are observed beneath the CMAP and NMAP. These low-velocity regions are seen throughout the rest of the period bands up to 100 s. A relatively strong low-velocity band at periods of 40–100 s is also apparent in southwestern Madagascar beneath the SMAP volcanic region. This anomaly appears to lie between two high-velocity zones and has a similar orientation to both the Davie Ridge and the Ranotsara shear zone.

4.3. Two-plane-wave tomography

To provide an analysis of the size of features resolvable by the TPW tomography method, a resolution matrix is calculated at each period and convolved with a checkerboard of positive and negative anomalies (Supplementary Fig. S5). For each period, multiple tests allow the determination of the smallest checker size that can be recovered by the resolution matrix. The shortest periods can resolve features 177 km in width, increasing to 355 km at the longest periods.

A subset of the resulting TPW 2D phase velocity maps are shown in Fig. 4. From 30 s to 77 s, two distinct relatively low-velocity zones underlie the CMAP and NMAP regions. A third low-velocity region underlies the SMAP region at periods of 40–77 s. The northern low-velocity region appears to remain disconnected from the central and southern regions at periods $<$124 s. These results show similar features to those of the ANT and ASWMS results: a central low-phase-velocity region correlates with the surface CMAP volcanics, a northern low-phase-velocity region correlates with the NMAP volcanics, and a southern low-phase-velocity region correlates with the SMAP volcanic region at periods $>$40 s.

4.4. Shear-velocity inversion

After amalgamating all of the 1-D model nodes, a 3-D model for the entire region with a 0.5° node spacing is obtained through interpolation (Supplementary Fig. S6). Depth slices are plotted relative to the mean of the slice to highlight the variations at each depth. In addition, slices relative to the Preliminary Reference Earth model (PREM) (Dziewonski and Anderson, 1981) are shown in Fig. 6 (the reference model is plotted in Supplementary Fig. S7

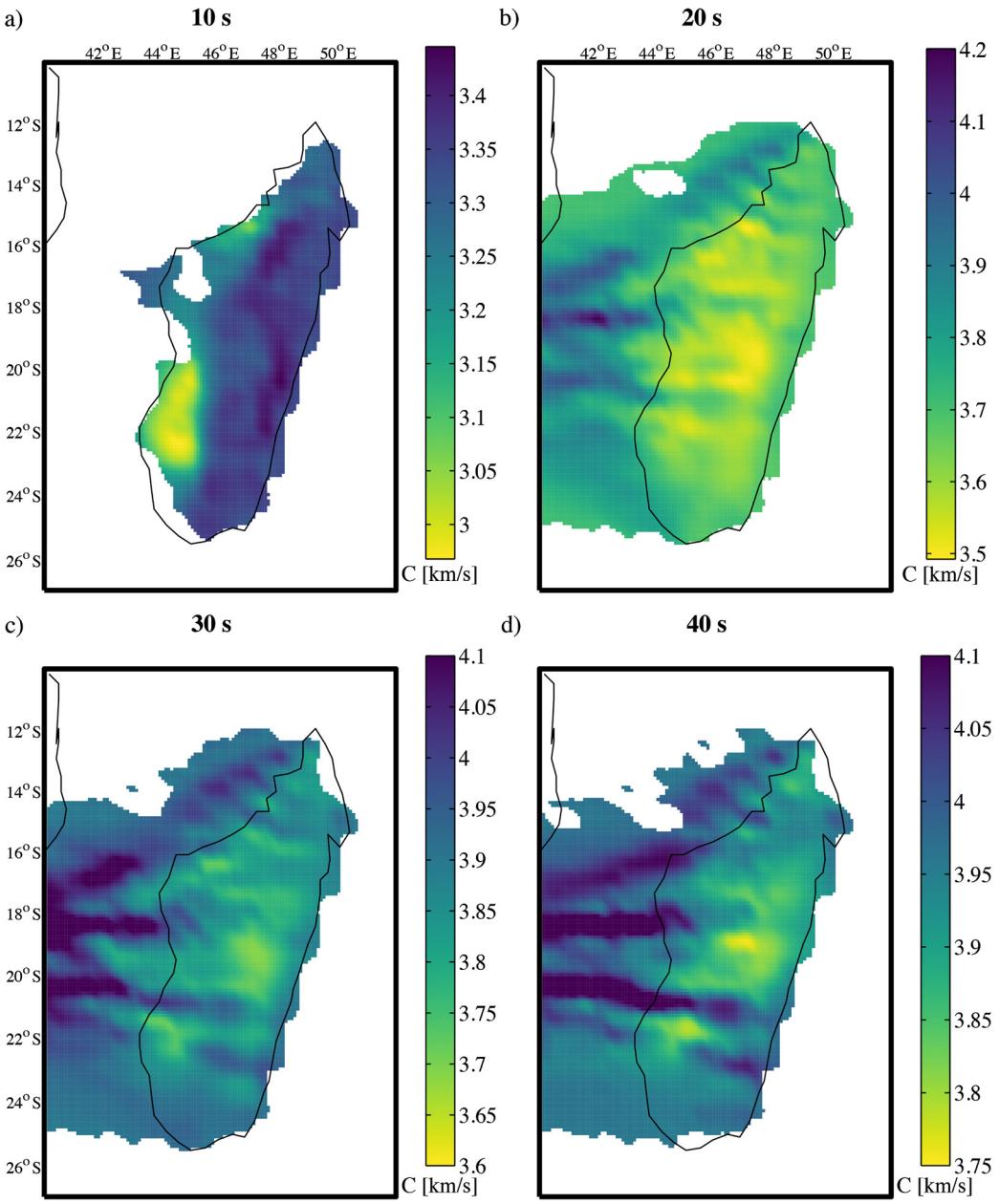

Fig. 2. Phase-velocity maps produced from the ANT method. Values are omitted where spatial resolution exceeds 200 km. Smearing between stations at longer periods is seen beneath the west coast due to a lack of crossing paths to island stations. Low phase-velocity regions at 10 s correlate with sedimentary basins. Velocity variations at 40 s also map well with respect to Madagascar volcanism. (For interpretation of the colors in this figure, the reader is referred to the web version of this article.)

and has been adapted within the top 40 km to highlight crustal variations).

Determining a shear-wave velocity model through a 1-D inversion at model nodes has limitations. For example, the velocities at each node are not directly influenced by the neighboring nodes. However, the smoothness of the final model suggests that the velocity variations observed are qualitatively robust. The RMS of the misfit between the inverted model dispersion curves and the final observed dispersion curves (Fig. 5) shows values less than 0.3 km/s across the majority of Madagascar rising to 0.6 km/s in the Mozambique Channel, where resolution is lost at shorter periods. The inclusion of an *a priori* Moho in the final round of inversion provides a more realistic velocity step at the base of the crust, and also shows a slight decrease when we include this Moho step (Fig. 5). The inferred Moho depth is relatively consistent with the surface topography: thickest throughout the Antananarivo terrane (~40–50 km), and thinning towards the west coast and to the north (~20–25 km) (Supplementary Fig. S8). However, alternative methods for determining crustal thickness other than surface wave phase velocities are beyond the scope of this paper.

Sedimentary basins are clearly observed as regions of relatively slow shear velocities along the west coast at 10 km in depth; the southern Morondava basin is the broadest and slowest (Supplementary Fig. S9). These shallow seismic structures are most sensitive to the ANT-method results, as both the ASWMS and TPW methods cannot resolve such short periods. The surface geologic boundary of sedimentary cover clearly separates the slow velocities of the sedimentary basins from the relatively fast Precambrian basement rocks to the east. In comparison, in the 30-km-deep map the color scheme inverts, showing relatively slow shear velocities along the backbone of the island and fast velocities to the west. This depth slice crosses an eastward-dipping Moho discontinuity, revealing the slow continental crustal root beneath the Madagascan highlands and fast mantle velocities beneath the Mozambique

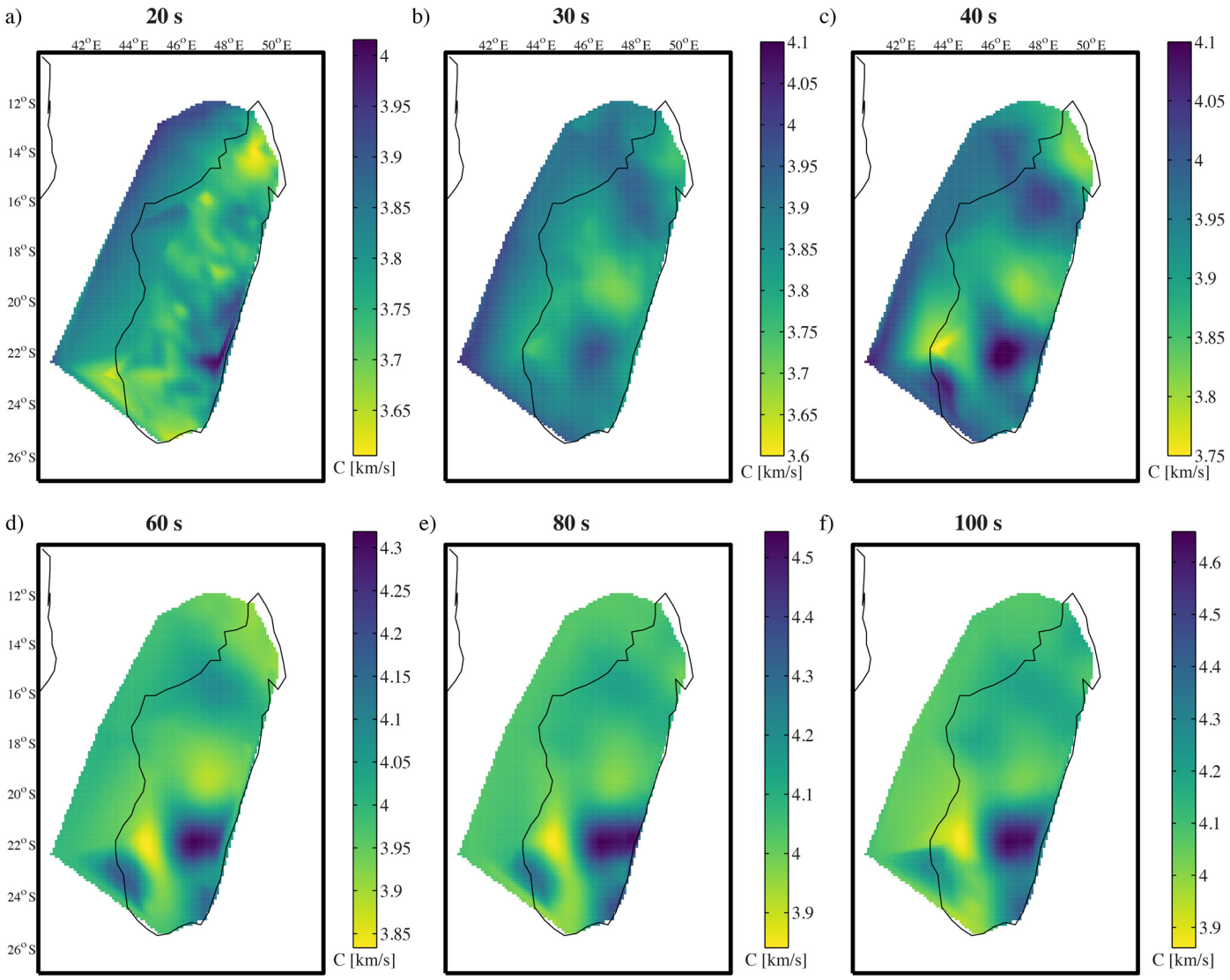

Fig. 3. Phase-velocity maps produced by the ASWMS method. These periods are mainly sensitive to the lower-crust and mantle velocity structure and show low-velocity regions that correlate well with the intraplate volcanism. At 20 s there is a clear variation in the Mozambique Channel velocities compared to those of Madagascar due to the faster, more oceanic-type crust. A third low-velocity region is observed in the southwest of Madagascar at longer periods. (For interpretation of the colors in this figure, the reader is referred to the web version of this article.)

Channel and shallow western Madagascar crust. In the upper mantle (50–150 km depth), three distinct low-velocity regions are observed beneath the NMAP, CMAP, and SMAP volcanic regions of the island. These low-shear-velocity regions are independent and unconnected at depths <100 km, although both the northern and central zones appear to migrate west and northwards with increasing depth.

5. Discussion

5.1. The crust

Shear-velocity variations across Madagascar show a variety of features that can be related to the surface geology. At shallow depths, the features that most stand out are the three west-coast sedimentary basins. These appear as the low-velocity anomalies in Fig. 2 and Fig. 5 at the shortest periods and shallowest depths. The Antsirinana Basin is the shallowest and narrowest of the three, and the Mahajanga Basin is deeper and broader, though both are likely to extend to less than 5 km in depth. The Morondava basin is by far the deepest and broadest of the three, and may be up to ~10 km deep (Supplementary Fig. S9). Surface waves are not the optimal means of measuring shallow basin structures, which are better resolved with receiver functions from *P* and *S* body waves, as well as active-source seismic methods. Receiver functions have been analyzed from the MACOMO data (Fenitra Andriampenomanana, pers. comm.) and show that the thickness of sedimentary rocks extends up to 8 km deep along the western edges of Madagascar, thinning to 3–6 km at their eastern boundary. The receiver functions suggest that the thickest sedimentary sequences are with the Morondava and Mahajanga Basins, but that even for the Antsirinana Basin to the north the sediment layers likely exceed 5 km. Nonetheless, the surface wave inversions show that the Morondava and Mahajanga Basins, and to a lesser degree the Antsirinana Basin, are major structural features that dominate the seismic structures of the Madagascan west coast.

At the shortest periods, the central mountainous spine of Madagascar is relatively fast in comparison to surrounding valleys. This is consistent with the crystalline Archaean rocks exposed there. The pattern of seismic velocities quickly reverses with depth, however, because of the slower seismic velocities of the Madagascan

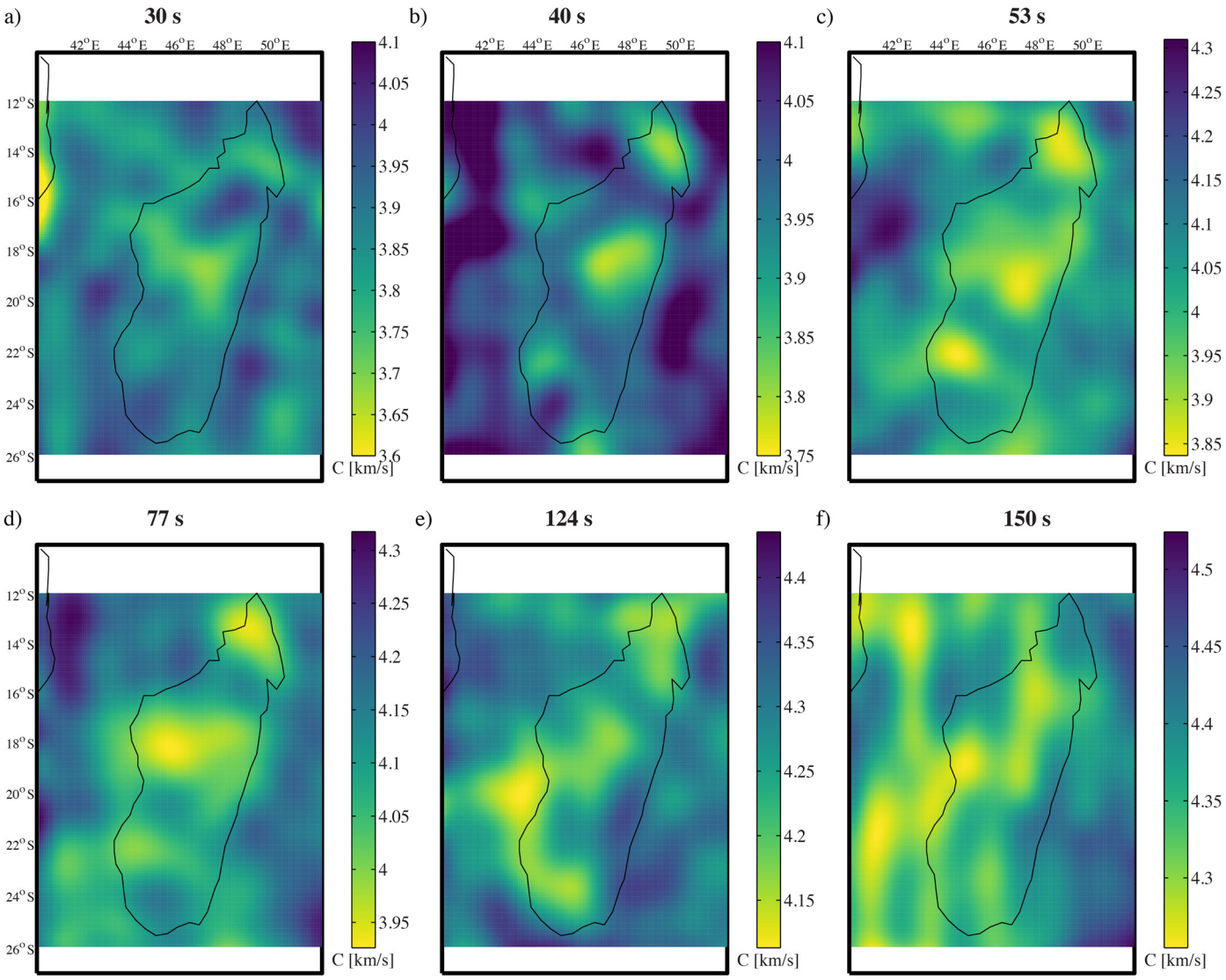

Fig. 4. A subset of phase-velocity maps produced by the TPW method. Two low-velocity zones again map beneath regions of intraplate volcanism. A third low-velocity region is also shown in the southwest of Madagascar at 40–70 s. It is noted that low-velocity regions appear to extend towards the Comoros, although the coverage in the Mozambique Channel is limited. (For interpretation of the colors in this figure, the reader is referred to the web version of this article.)

Highlands continental root in comparison to the mantle velocities beneath the thinned crust of the west-coast basins. This is clearly observed in the transition between 10 and 50 km (Fig. 6 and Supplementary Fig. S6): at 10 km depth, the Morondava basin appears as a large low-velocity feature because of the very thick sedimentary basin that formed syntectonically as Madagascar was rifting away from Africa. However, at 30-km-depth, these anomalies have begun to reverse. The N–S mountains are still continental crustal material, whereas beneath the Morondava basin, where the crustal thickness is likely around 23–33 km (Fenitra Andriampenomanana, pers. comm.), the thin crust may have been replaced by denser and seismically faster mantle rock.

The Moho depths are estimated by applying a jump in shear velocity at 4.125 km/s. This approach works well in allowing the inversion to generate a more reasonable velocity model. However, in the CMAP it is likely that the Moho depth is misplaced, as the inversion attempts to reduce the velocity jump applied to the smoothed model during the second round of iterations (Supplementary Fig. S8b). To the degree that the 1-D models within the CMAP area produce a low-shear-velocity zone (<4.2 km/s) at upper mantle depths, the depth range that a suitable Moho could exist increases. As such, caution is needed when interpreting the crustal thickness measurements, particularly within the CMAP region.

5.2. The upper mantle

The dominant seismic anomalies just below the crust are two regions of very slow seismic velocities at the top of the upper mantle. These anomalies are best seen in the deeper maps of the joint model (Fig. 5d and 5e) and in the cross-sections of the relative shear-velocity model (Fig. 7), which has been saturated at a minimum of 4.1 km/s in order to observe the much smaller mantle anomalies. The two upper mantle slow-velocity anomalies are observed beneath the central and northern regions of the island. These anomalies directly underlie the locations of known recent volcanic activity of the CMAP and the NMAP regions. At depths of 80–100 km a negative shear-velocity anomaly of around −4% is observed relative to PREM (Fig. 6). This is consistent with other such anomalies at these depths, where there is little or no mantle lithosphere (e.g., Petit et al., 2008).

A third notable low-velocity region is situated to the south of the island at depths of 50–100 km (Fig. 7C–C'). This feature appears separated from the CMAP low-velocity region at depths of

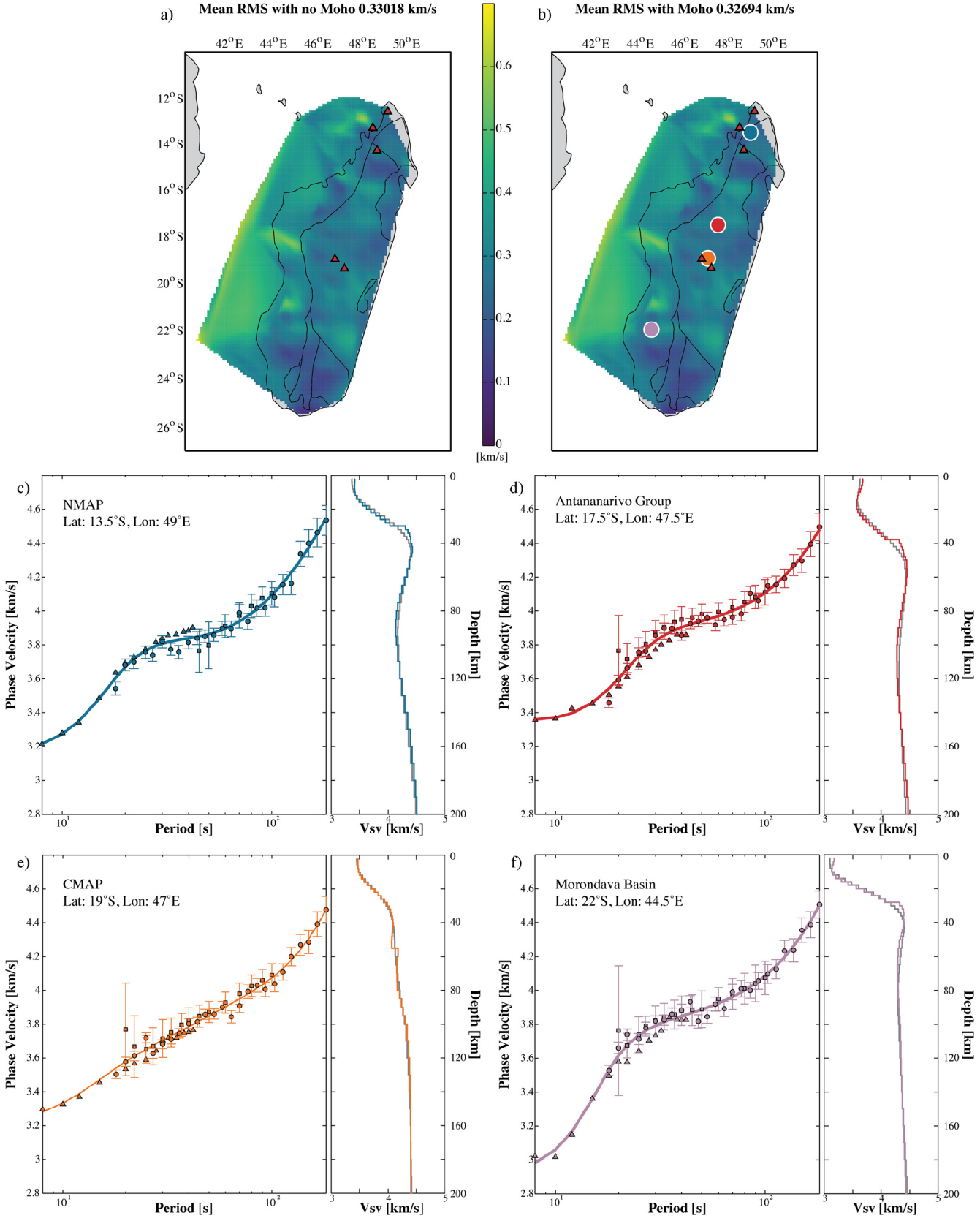

Fig. 5. Maps of RMS shear-velocity between observed and modeled dispersion for both the initial smooth inversion (a) and the secondary inversion that includes a Moho discontinuity at 4.125 km/s (b). Selected phase-velocity dispersion observations and modeled dispersion curves and the corresponding 1-D shear-velocity inversion (c–f) at locations marked on (b). Gray lines denote the smooth model inversion and the colored lines display the secondary inversion. Marker symbols denote method used for the phase-velocity measurement: ANT (triangles), ASWMS (squares) and TPW (circles). Tectonic boundaries and recent volcanoes are marked as previous. Locations are chosen based on geologic diversity: Antananarivo Group – Precambrian metamorphic basement showing relative fast phase velocities at short periods and thick (~35–40 km) crust; Morondava Basin – slow phase velocities at short periods due to sedimentary cover; NMAP – northern volcanic region; CMAP – central volcanic region showing significantly slower phase-velocity observations at intermediate periods. (For interpretation of the colors in this figure, the reader is referred to the web version of this article.)

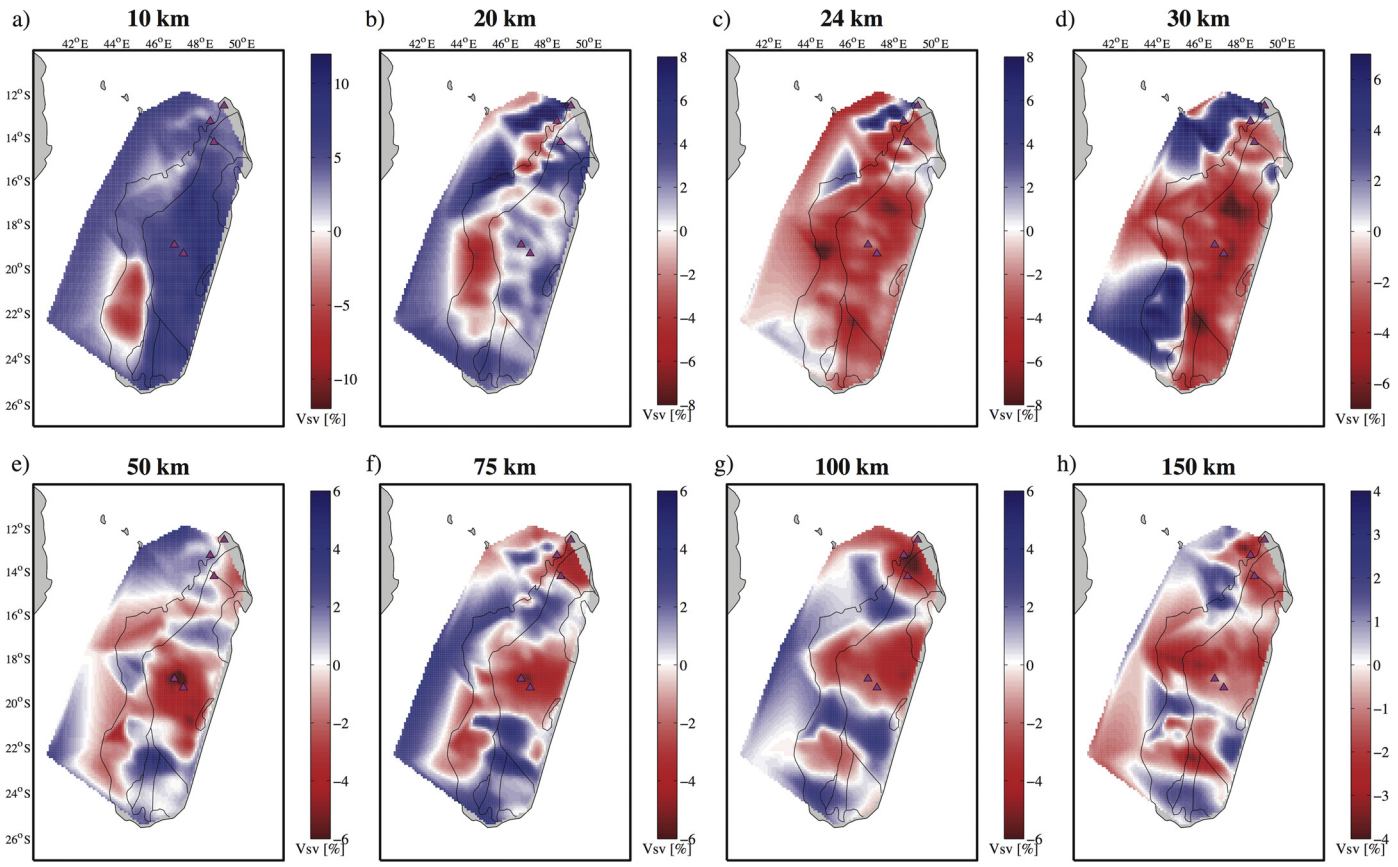

Fig. 6. Relative shear velocities with respect to PREM. The reference model has been modified in the top 40 km (Supplementary Fig. S7) in order to highlight velocity variations such as sedimentary basins and Moho topography. The absolute velocity model is shown in Supplementary Fig. S6. (For interpretation of the colors in this figure, the reader is referred to the web version of this article.)

75–150 km by a zone of fast shear velocity (~4.5 km/s, Fig. 6f–h, 7C–C' and D–D'), although there may be some low velocity connection to the western edge of the CMAP low-velocity region at ~50 km (Fig. 6e). It is also noted that this low-velocity region lies beneath the outcrop of Cenozoic volcanic rocks at Ankilioaka, which have been dated at ~9 Ma (Bardintzeff et al., 2010).

5.3. Regional interpretation of upper mantle low velocity zones

The extension of these low-velocity anomalies to depths greater than 150 km requires additional techniques such as the inclusion of body-wave tomography, and it is therefore unclear as to whether these low-velocity regions are the result of active or passive upwelling. Global models in this particular region are too course to see any fine detail that is required to help resolve this issue. Nonetheless, the structures that are resolvable can begin to allow some inferences as to the source or sources of Madagascar's intraplate volcanism. For example, fast phase velocities at long periods (40–100 s, Fig. 3) and great depths (50–100 km; see Fig. 7 D–D') beneath the region just to the south of the CMAP may suggest the delamination and removal of mantle lithosphere through negative buoyancy forces. The removal of sub-CMAP mantle lithosphere would allow for the replacement by asthenospheric mantle rising beneath the CMAP. Subsequent isostatic adjustment would result in elevated topography that is observed along the backbone of Madagascar. An alternative hypothesis to the existence of these low shear velocities would be the presence of remnants of Cretaceous hotspot activity from the Marion hotspot (Torsvik et al., 1998). However, current active uplift rates inferred from river profiles (Roberts et al., 2012) suggest that the high topography is a recent feature, more likely resulting from the thermal uplift of more recently emplaced sub-lithospheric low-density rocks. The presence of low velocity mantle beneath the SMAP region may provide an explanation to the relatively high topography of the Morondava basin (Fig. 1, Supplementary Fig. S9). Further modeling of dynamic topography is required, and river profile records appear to show that topography in the Morondava basin also may have developed since 8 Ma.

If there is a connection at depth to an active plume source, the most likely direction is from the Comoros volcanic alignment to the northwest. Recent analysis has suggested that the Comoros volcanic alignment is not related to a deep mantle hotspot (Michon, 2016). The emerging idea is that volcanism and areas of high heat flow in this region are strongly related to African tectonics. The central and northern low-velocity anomalies are clearly distinct from each other at shallow depths, separated by a strong and deep fast-velocity region. There does not appear to be any sub-lithospheric flow connecting these two regions. The velocity model loses resolution to the east of Madagascar, but at its deepest, the model displays a possible low-velocity region extending northwest from both the north and central regions, possibly connecting them with the Comoros region. This would be in agreement with an African plume-source model (Ebinger and Sleep, 1998; Nyblade et al., 2000; Lin et al., 2005), which involves having a central plume beneath East-Central Africa spread out beneath the African lithosphere, supplying the magma for other shallow, regional hot spot volcanoes. In the Ebinger and Sleep (1998) model, plume material flows shallowly beneath the lithosphere and comes from the northwest, suggesting that volcanism began in the Comoros and the NMAP before the more southerly CMAP (as the leading edge of the plume material moved southeastward from Kenya/Tanzania). In the Forte et al. (2010) model, plume mate-

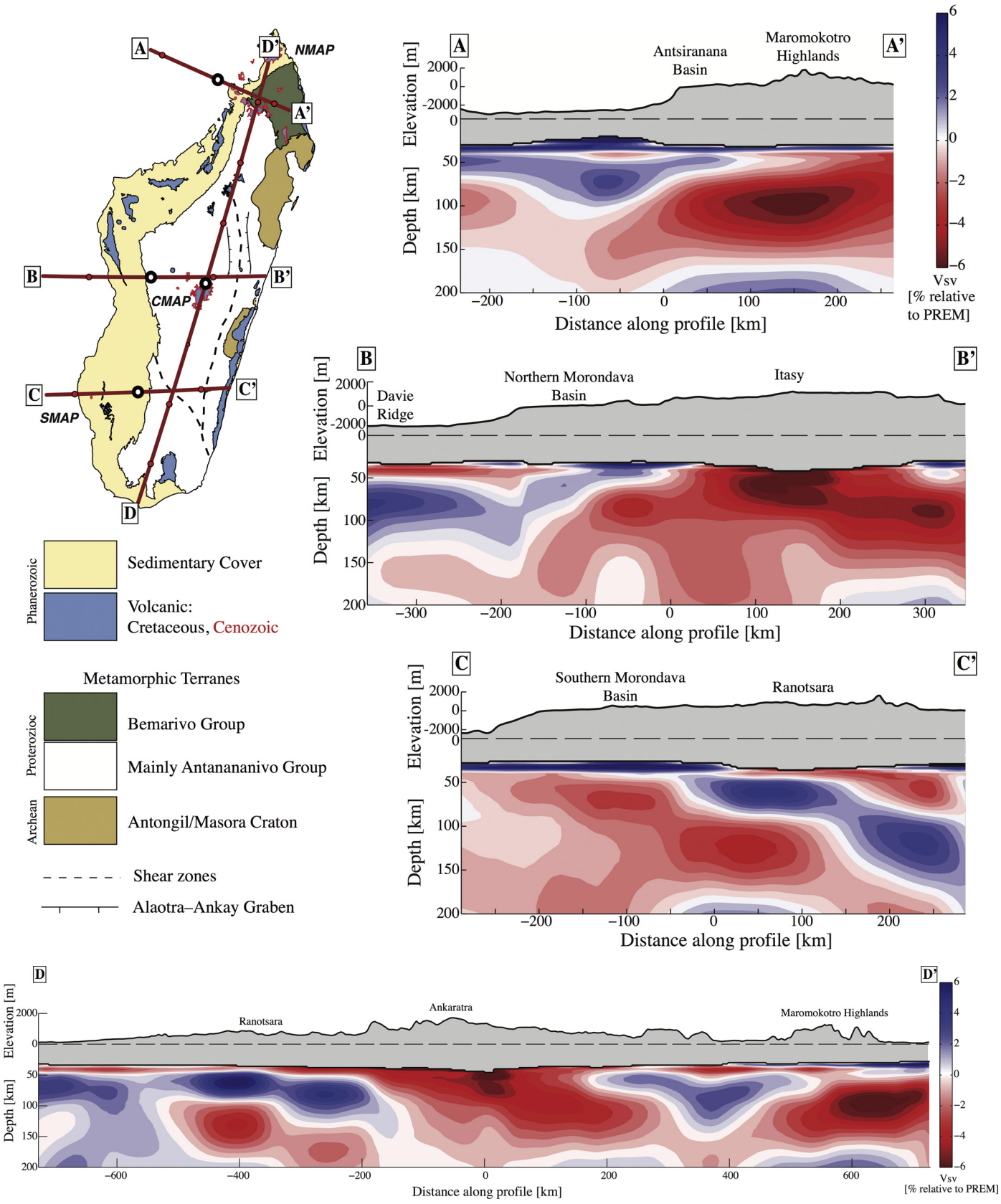

Fig. 7. Cross-sections through the shear-velocity model with respect to PREM shown in Fig. 6 to 200 km depth. Sections are shown on the geologic map, white circles mark the 0 km position of the profiles, and red circles are at 200 km intervals. Vertically exaggerated elevation profiles are shown based on ETOPO1 (Amante and Eakins, 2009), and the dashed line marks the change in scale. The color scale is consistent for all cross-sections. Upper-mantle low-velocity regions are observed beneath higher-elevated areas and specifically beneath regions of Cenozoic volcanism (A–A', B–B'). Profile C–C' traverses southern Madagascar where, at the southwestern end beneath the SMAP, lies an upper-mantle low-velocity region that is observable at 50 km in depth, but becomes much stronger with greater depth. (For interpretation of the colors in this figure, the reader is referred to the web version of this article.)

rial is proposed to rise from beneath south Africa and to spread towards the NE beneath the western Indian Ocean. This suggests that the Madagascar volcanism is not directly generated by an upwelling source beneath the Comoros entrained by the mantle flow but instead, that both volcanism could represent the effects of the southern termination of the East African Rift, as proposed by Michon (2016).

An active upwelling source is not ruled out with the limited geochemical studies on the volcanic regions. Bardintzeff et al. (2010) conclude that the Madagascar volcanic regions may indeed share a similar source but with differing levels of crustal mixing. The northern volcanic rocks may exhibit a slightly more depleted signature than the central volcanics, but all could be attributed to an ocean island basalt source. The enrichment in trace elements for the recent CMAP and NMAP, as well as the small SMAP region, is about double that of the older, 93.5 Ma volcanic rocks from the Morondava basin, which are from the Marion hotspot (Wen, 2006).

In response to inadequacies in the Emerick and Duncan (1982) model, Nougier et al. (1986) proposed a fracture-zone model that relied on the reactivation of remnant faults and shear zones formed by tectonic processes as Madagascar rifted away from Africa. This model allows for the passage of alkali-enriched material to be concentrated along zones parallel to the Davie Ridge. Although this model allows for a connection to the Comorean plume, it does not discount the idea that the source could be a more localized upwelling, possibly in the form of metasomatized mantle enriched in incompatible elements (e.g., Pilet et al., 2004). The results here do not discount this hypothesis; however, it seems that current extension rates within Madagascar and the deep nature of the low-velocity anomalies makes this model less likely.

From the shear-velocity model proposed here, we interpret the high elevations of the Madagascan highlands to be due to a thin, and even absent, mantle lithosphere beneath an average-thickness (40 km) continental crust. The cause of this thinning appears to be much more than the current extensional stress regime allows. Thermo-mechanical removal of mantle lithosphere may provide an alternative hypothesis to explain our shear velocities, but also the recent dynamic uplift of topography, and the negative Bouguer gravity anomaly (Bonvalot et al., 2012). The presence of delaminated, cold lithosphere at depths below 150 km could potentially be imaged using receiver functions and regional body wave tomography.

6. Conclusions

Surface-wave-derived phase-velocity data have, for the first time, allowed a more detailed interpretation of shear velocities in the crust and upper mantle beneath Madagascar. Sedimentary basins are observed to extend to depths of around 10 km beneath the west coast using these surface-wave methods, in agreement with other body-wave based studies. Regions of low upper-mantle shear velocities are shown to lie beneath both the CMAP and NMAP, the locations of recent intraplate volcanism. A third low-velocity region lies at upper mantle depths beneath the SMAP in the southwestern region of Madagascar and appears not to extend up into the crust. Any deeper connections among these low-velocity regions and their extensions into the mantle transition zone cannot be interpreted using surface-wave methods employed here. The elevated topography of the Madagascar highlands around the CMAP may be explained by buoyant, low-velocity asthenosphere. The cause of this feature can be explained by the localized removal of mantle lithosphere beneath the CMAP allowing sublithospheric mantle to flow in from the north, however, we do not rule out a deeper source of mantle heating. Body-wave tomography and anisotropy studies will lend evidence to help explain the occurrence of these low-velocity regions and the potential for an active, deep-rooted source.

Acknowledgements

We thank Peter Shearer, Nathan Simmons and one anonymous reviewer for providing productive comments that helped improve this manuscript. We would like to acknowledge the IRIS/PASSCAL instrument center for providing instrumentation for the MACOMO project. The Missouri Botanical Gardens provided invaluable guidance regarding site selection and security. Thanks also go to Frederik Tilmann and Karin Sigloch for providing additional datasets and comments, and to Franklin Koch for help deploying stations. Funding for the MACOMO project was provided by NSF award EAR-0838426. RHUM-RUM seismological deployments were supported by the French CNRS-INSU (Institut National des Sciences de l'Univers), program SYSTER, by the CNRS-INEE (Institut National Ecologie et Environnement), the TAAF (Terres Australes et Antarctiques Françaises), by the French ANR (Agence Nationale de la Recherche, project ANR-11-BS56-0013), and by the DFG (Deutsche Forschungsgemeinschaft) grant SI1538/2-1 RHUM-RUM in Germany. RHUM-RUM equipments were provided by the Alfred Wegener Institut (AWI) in Bremerhaven, Germany, and by RESIF-SISMOB in Grenoble, France.

Appendix A. Supplementary material

Supplementary material related to this article can be found online at http://dx.doi.org/10.1016/j.epsl.2016.10.041.

References

Amante, C., Eakins, B.W., 2009. ETOPO1 1 Arc-Minute Global Relief Model: Procedures, Data Sources and Analysis. NOAA technical memorandum NESDIS NGDC-24. National Geophysical Data Center, NOAA.

Bardintzeff, J-M., Liegeois, J-P., Bonin, B., Bellon, H., Rasamimanana, G., 2010. Madagascar volcanic provinces linked to the Gondwana break-up: geochemical and isotopic evidences for contrasting mantle sources. Gondwana Res. 18, 295–314.

Barmin, M.P., Ritzwoller, M.H., Levshin, A.L., 2001. A fast and reliable method for surface wave tomography. Pure Appl. Geophys. 158, 1351–1375.

Barruol, G., Sigloch, K. RHUM-RUM group 2012. RHUM-RUM experiment, 2011–2015, code YV (Réunion Hotspot and Upper Mantle – Réunion's Unterer Mantel) funded by ANR, DFG, CNRS-INSU, IPEV, TAAF, instrumented by DEPAS, INSU-OBS, AWI and the Universities of Muenster. Bonn, La Réunion; RESIF – Réseau Sismologique et géodésique Français. http://dx.doi.org/10.15778/RESIF.YV2011.

Bensen, G.D., Ritzwoller, M.H., Barmin, M.P., Levshin, A.L., Lin, F-C., Moschetti, M.P., Shapiro, N.M., Yang, Y., 2007. Processing seismic ambient noise data to obtain reliable broad-band surface wave dispersion measurements. Geophys. J. Int. 169, 1239–1260.

Bonvalot, S., Balmino, G., Briais, A., Kuhn, M., Peyrefitte, A., Vales, N., Biancale, R., Gabalda, G., Moreaux, G., Reinquin, F., Sarrailh, M., 2012. World Gravity Map, 1:50000000 map, Eds.: BGI-CGMW-CNES-IRD, Paris. ©CGMW-BGI-CNES-IRD.

Chevrot, S., et al., 2014. High-resolution imaging of the Pyrenees and Massif Central from the data of the PYROPE and IBERARRAY portable array deployments. J. Geophys. Res., Solid Earth 119, 6399–6420.

Coffin, M.F., Rabinowitz, P.D., 1987. Reconstruction of Madagascar and Africa: evidence from the Davie Fracture Zone and Western Somali Basin. J. Geophys. Res. 92. http://dx.doi.org/10.1029/JB092iB09p09385.

Collins, A.S., 2006. Madagascar and the amalgamation of Central Gondwana. Gondwana Res. 9, 3–16.

Cox, R., Zentner, D.B., Rakotondrazafy, A.M., Rasoazanamparany, C.F., 2010. Shakedown in Madagascar: occurrence of lavakas (erosional gullies) associated with seismic activity. Geology 38 (2), 179–182.

Dziewonski, A.M., Anderson, D.L., 1981. Preliminary reference Earth model. Phys. Earth Planet. Inter. 25, 297–356.

Ebinger, C.J., Sleep, N.H., 1998. Cenozoic magmatism throughout east Africa resulting from impact of a single plume. Nature 395, 788–791.

Emerick, C.M., Duncan, R.A., 1982. Age progressive volcanism in the Comores Archipelago, western Indian Ocean and implications for Somali plate tectonics. Earth Planet. Sci. Lett. 60, 415–428.

Forsyth, D.W., Li, A., 2005. Array analysis of two-dimensional variations in surface wave phase velocity and azimuthal anisotropy in the presence of multipathing

interference. In: Levander, A., Nolet, G. (Eds.), Seismic Earth: Array Analysis of Broadband Seismograms. American Geophysical Union, Washington, D.C.
Forte, A.M., Quéré, S., Moucha, R., Simmons, N.A., Grand, S.P., Mitrovica, J.X., Rowley, D.B., 2010. Joint seismic–geodynamic–mineral physical modelling of African geodynamics: a reconciliation of deep-mantle convection with surface geophysical constraints. Earth Planet. Sci. Lett. 295, 329–341.
Fourno, J.-P., Roussel, J., 1994. Imaging of the Moho depth in Madagascar through the inversion of gravity data: geodynamic implications. Terra Nova 6, 512–519.
Gibbons, A.D., Whittaker, J.M., Müller, R.D., 2013. The breakup of East Gondwana: assimilating constraints from Cretaceous ocean basins around India into a best-fit tectonic model. J. Geophys. Res., Solid Earth 118, 808–822.
Grimison, N.L., Chen, W-P., 1988. Earthquakes in the Davie Ridge-Madagascar region and the southern Nubian–Somalian plate boundary. J. Geophys. Res. 93. http://dx.doi.org/10.1029/JB093iB09p10439.
Herrmann, R.B., Ammon, C.J., 2002. Computer Programs in Seismology Version 3.20: Surface Waves, Receiver Functions, and Crustal Structure. St. Louis University, Missouri. Available at http://mnw.eas.slu.edu/People/RBHerrmann.
Jin, G., Gaherty, J.B., 2015. Surface wave phase-velocity tomography based on multichannel cross-correlation. Geophys. J. Int. 201, 1383–1398.
Kennett, B.L.N., Engdahl, E.R., Buland, R., 1995. Constraints on seismic velocities in the Earth from traveltimes. Geophys. J. Int. 122, 108–124.
Larose, E., Derode, A., Clorennec, D., Margerin, L., Campillo, M., 2005. Passive retrieval of Rayleigh waves in disordered elastic media. Phys. Rev. E 72, 046607.
Laske, G., Masters, G., Ma, Z., Pasyanos, M., 2013. Update on CRUST1.0 – A 1-degree global model of Earth's crust. In: EGU General Assembly.
Levshin, A.L., Ratnikova, L., Berger, J., 1992. Peculiarities of surface wave propagation across Central Eurasia. Bull. Seismol. Soc. Am. 82, 2464–2493.
Li, A., Burke, K., 2006. Upper mantle structure of southern Africa from Rayleigh wave tomography. J. Geophys. Res. 111, B10303. http://dx.doi.org/10.1029/2006JB004321.
Lin, S-C., Kuo, B-Y., Chiao, L-Y., van Keken, P.E., 2005. Thermal plume models and melt generation in East Africa: a dynamic modeling approach. Earth Planet. Sci. Lett. 237, 175–192.
Michon, L., 2016. The volcanism of the Comores archipelago integrated at a regional scale. In: Bachèlery, P., Lénat, J.-F., Di Muro, A., Michon, L. (Eds.), Active Volcanoes of the Southwest Indian Ocean: Piton de la Fournaise and Karthala. Active Volcanoes of the World. Springer-Verlag, Berlin, Heidelberg, pp. 333–344.
Nougier, J., Cantagrel, J.M., Karche, J.P., 1986. The Comores archipelago in the western Indian Ocean: volcanology, geochronology and geodynamic setting. J. Afr. Earth Sci. 5, 135–144.
Nyblade, A.A., Owens, T.J., Gurrola, H., Ritsema, J., Langston, C.A., 2000. Seismic evidence for a deep upper mantle thermal anomaly beneath East Africa. Geology 28, 599–602.
Pacquette, J-L., Moine, B., Rakotondrazafy, M., 2003. ID-TIMS using the step-wise dissolution technique versus ion microprobe U–Pb dating of metamict Archean zircons from NE Madagascar. Precambrian Res. 121, 523–538.
Petit, C., Tiberi, C., Deschamps, A., Déverchère, J., 2008. Teleseismic traveltimes, topography and the lithospheric structure across central Mongolia. Geophys. Res. Lett. 35, L11301. http://dx.doi.org/10.1029/2008GL033993.
Pilet, S., Hernandez, J., Bussy, F., Sylvester, P.J., 2004. Short-term metasomatic control of Nb/Th ratios in the mantle sources of intra-plate basalts. Geology 32, 113–116.
Rabinowitz, P.D., Coffin, M.F., Falvey, D., 1983. The separation of Madagascar and Africa. Science 220 (4592), 67–69.
Rakotondraompiana, S.A., Albouy, Y., Piqué, A., 1999. Modèle de lithosphère pour l'île de Madagascar (océan Indien occidental): nouvelle interprétation des données gravimétriques. J. Afr. Earth Sci. 28, 961–973.
Rindraharisaona, E.J., Guidarelli, M., Aoudia, A., Rambolamanana, G., 2013. Earth structure and instrumental seismicity of Madagascar: implications on the seismotectonics. Tectonophysics 594, 165–181. http://dx.doi.org/10.1016/j.tecto.2013.03.033.
Ritzwoller, M.H., Shapiro, N.M., Levshin, A.L., Bergman, E.A., Engdahl, E.R., 2003. Ability of a global three-dimensional model to locate regional events. J. Geophys. Res. 108 (B7), 2353. http://dx.doi.org/10.1029/2002JB002167.
Roberts, G.G., Paul, J.D., White, N., Winterbourne, J., 2012. Temporal and spatial evolution of dynamic support from river profiles: a framework for Madagascar. Geochem. Geophys. Geosyst. 13, Q04004. http://dx.doi.org/10.1029/2012GC004040.
Roig, J.Y., Tucker, R.D., Delor, C., Peters, S.G., Théveniaut, H., 2012. Carte géologique de la Répulique de Madagascar à 1/1000000. Ministère des Mines, PGRM, Antananarivo, République Madagascar, 1 Color sheet.
Saria, E., Calais, E., Stamps, D.S., Delvaux, D., Hartnady, C., 2014. Present-day kinematics of the East African Rift. J. Geophys. Res. 119, 3584–3600.
Shapiro, N.M., Campillo, M., 2004. Emergence of broadband Rayleigh waves from correlations of the ambient seismic noise. Geophys. Res. Lett. 31. http://dx.doi.org/10.1029/2004GL019491.
Stamps, D.S., Iaffaldano, G., Calais, E., 2015. Role of mantle flow in Nubia–Somalia divergence. Geophys. Res. Lett. 42, 290–296.
Storey, M., Mahoney, J.J., Saunders, A.D., Duncan, R.A., Kelley, S.P., Coffin, M.F., 1995. Timing of hotspot related volcanism and breakup of Madagascar and India. Science 267, 852–855.
Tilmann, F., Yuan, X., Rümpker, G., Rindraharisaona, E., 2012. SELASOMA project, Madagascar 2012–2014. Deutsches GeoForschungsZentrum GFZ. Seismic Network. http://dx.doi.org/10.14470/MR7567431421.
Torsvik, T.H., Tucker, R.D., Ashwal, L.D., Eide, E.A., Rakotosolofo, N.A., de Wit, M.J., 1998. Late Cretaceous magmatism in Madagascar: paleomagnetic evidence for a stationary Marion hotspot. Earth Planet. Sci. Lett. 64, 221–232.
Tucker, R.D., Conrad, J., 2008. $^{40}Ar/^{39}Ar$ geochronology of Mesozoic and younger igneous rocks of central and northern Madagascar. Final report of the BGS-USGS Consortium to the Government of Madagascar, World Bank Project UK-04-0100, Chapter 7.
Tucker, R.D., Kusky, T.M., Buchwaldt, R., Handke, M.J., 2007. Neoproterozoic nappes and superimposed folding of the Itremo Group, west-central Madagascar. J. Gondwana Res. 12, 32–56.
Tucker, R.D., Roig, J-Y., Macey, P.Y., Delor, C., Amelin, Y., Armstrong, R.A., Rabarimanana, M.H., Ralison, A.V., 2011. A new geological framework for south-central Madagascar, and its relevance to the "out-of-Africa" hypothesis. Precambrian Res. 185, 109–130.
Wen, L., 2006. A compositional anomaly at the Earth's core–mantle boundary as an anchor to the relatively slowly moving surface hotspots and as source to the DUPAL anomaly. Earth Planet. Sci. Lett. 246, 138–148.
Wysession, M.E., Wiens, D.A., Nyblade, A.A., 2011. Investigation of sources of intraplate volcanism using PASSCAL broadband instruments in Madagascar, The Comores, and Mozambique. International Federation of Digital Seismograph Networks. Other/Seismic Network. http://dx.doi.org/10.7914/SN/XV_2011.
Yang, Y., Forsyth, D.W., 2006. Regional tomographic inversion of the amplitude and phase of Rayleigh waves with 2-D sensitivity kernels. Geophys. J. Int. 166, 1148–1160.